Zaheeruddin; Manas, Munish

Article

Renewable energy management through microgrid central controller design: An approach to integrate solar, wind and biomass with battery

Energy Reports

Suggested Citation: Zaheeruddin; Manas, Munish (2015) : Renewable energy management through microgrid central controller design: An approach to integrate solar, wind and biomass with battery, Energy Reports, ISSN 2352-4847, Elsevier, Amsterdam, Vol. 1, pp. 156-163, https://doi.org/10.1016/j.egyr.2015.06.003

Energy Reports 1 (2015) 156–163

Contents lists available at ScienceDirect

Energy Reports

journal homepage: www.elsevier.com/locate/egyr

Renewable energy management through microgrid central controller design: An approach to integrate solar, wind and biomass with battery

Zaheeruddin [1], Munish Manas *

Department of Electrical Engineering, Faculty of Engineering and Technology, Jamia Millia Islamia (A Central University), New Delhi 110025, India

ARTICLE INFO

Article history:
Received 14 January 2015
Received in revised form
24 April 2015
Accepted 22 June 2015
Available online 17 July 2015

Keywords:
Microgrid
Microgrid central controller (MGCC)
Energy management
Renewable energy sources modeling

ABSTRACT

In this study, an isolated microgrid comprising of renewable energy (RE) sources like wind, solar, biogas and battery is considered. Provision of utility grid insertion is also given if total microgrid sources falls short of supplying the total load. To establish an efficient energy management strategy, a central controller takes the decision based on the status of the loads and sources. The status is obtained with the assistance of multi-agent concept (treating each source and load as an agent). The data acquisition system of these renewable sources and loads consists of multiple sensors interconnected through Low Power Radio over one of many GPRS communication. The Microgrid Central Controller (MGCC) would use an embedded energy management algorithm to take decisions, which are then transmitted to the controllable RE systems to manage the utilization of their power outputs as per the load-supply power balance. A control strategy is adopted to regulate the power output from the battery in case of supply shortage, which results in a floating battery scheme in steady state.

1. Introduction

In today's world, the reduction of greenhouse gas emission from the conventional thermal power plants is quite necessary. For the reduction of greenhouse gases from the electrical power sources, the power producers are now marching towards usage of renewable energy sources (RESs) (Bull, 2001). A study on the US power system suggests that a conservative approach could reduce annual CO_2 emissions by 5% by 2030 (Hledik, 2009). Also, if the national electricity market were to function properly, the renewable energy technologies would offer the cheapest forms of power generation (Sovacool, 2008). In general, these sources are small in capacity and thus are mostly connected at distribution voltage level and are known as distributed generation (DG). This localized grouping of electricity generation, storage, and loads that normally operate connected to a centralized utility grid is called as a microgrid (Mishra et al., 2012). In reality there are technical limits on the degree to which distributed generation can be connected, especially for some intermittent forms of renewable generation (Arulampalam et al., 2004).

In this study a microgrid comprising of controllable renewable sources like wind, solar, biogas and battery is considered for supplying the load. In a microgrid (Valenciaga and Puleston, 2005) the power output from controllable sources changes, thus they have to be regulated. The solution is to have a battery with state of charge (SOC) greater than 20% to bridge the gap between the power produced by the RESs and loads. As per SOC of battery and real power needs of the microgrid, the battery is either charged or discharged (Xu et al., 2012). If the SOC of battery is less than 20% then utility grid has to be inserted as the last resort to meet the deficit load. The battery control mechanism should also consider its SOC to avoid any damage due to overcharging (Miao et al., 2014). Thus, in line with the literature review of State of charge of the batteries used for microgrid integration, the SOC limit for operation has been kept between 20% and 80% (Prajapati et al., 2011). Here, we are managing the output power available from different microgrid energy sources to maintain microgrid load–source power balance. The battery used for supplying the deficit power (in case renewable energy sources are insufficient to meet the load) is integrated here. Even though a battery is a highly reliable power source, it cannot be used under steady state for power exchange with the microgrid. Thus, a battery power control mechanism for handling load fluctuations is implemented (Bragard et al., 2010; Vazquez et al., 2010).

The microgrid has a larger power capacity and more control flexibilities to fulfill system reliability and power quality requirements (Gaonkar, 2010). The features of the microgrid can improve the reliability of the power supply but it also creates specific problems like transient dynamics, Intermittency of renewables, load

* Corresponding author. Tel.: +91 9971927385.
E-mail addresses: zaheeruddin@jmi.ac.in (Zaheeruddin), msd.gkg85@gmail.com (M. Manas).
[1] Tel.: +91 9910170032.

http://dx.doi.org/10.1016/j.egyr.2015.06.003

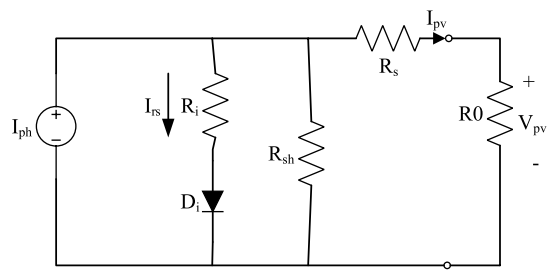

Fig. 1. Solar PV panel equivalent circuit.

management, reliability issues etc. The problem of transient dynamics is fundamentally important because it concerns the protection configuration, control strategy formulation, and transient stability assessment of the whole power system (Xiong and Ouyang, 2011). In this study, we are considering how to improve the transient dynamics by designing a microgrid central controller.

The exact objective of this study is to formulate and implement an energy management algorithm for supplying reliable power to the connected load in a microgrid, by designing a microgrid central controller (MGCC). Such a controller finds its usefulness in managing intermittency of power supply from renewable energy sources in a microgrid set up and is of immense use to the distribution utility and microgrid energy management sector. Due to higher sampling rate of MGCC, it can handle both primary as well as secondary controllers. For effective resource utilization and control of microgrid power sources a smart MGCC is developed based on multi agent system (MAS) concept. The renewable energy sources considered for this study are solar photovoltaic (PV), wind energy, and biogas internal combustion engine. The data acquisition system of these renewable sources and loads consists of multiple sensors interconnected through Low Power Radio (LPR) (http://www.fi-ppp-finseny.eu/wp-content/uploads/2013/04/FINSENY_D3\T1\ndash3_Microgrid_Functional_Architecturev1_0_March_2013.pdf). The data thus received will be utilized by MGCC for deciding the control actions. The microgrid proposed in this study is with the following installed capacities: (a) Wind Gen.—40 kW, (b) Solar photovoltaic Generation.—13 kW_p, (c) Biogas Generation—25 kW, (d) Total Load—80 kW, (e) Battery I.C.—200 kWh.

This paper is organized in the following manner. Section 2 describes the modeling of renewable energy sources. Section 3 presents the formulation of energy management algorithm. Section 4 illustrates the modeling and design of Microgrid Central Controller (MGCC). Section 5 demonstrates the simulation results and analysis. Section 6 presents the conclusion.

2. Modeling and simulation of renewable energy sources and the battery

In order to verify the correct functioning of the designed Microgrid Central Controller, a dynamic model of the proposed microgrid system is necessary. The modeling of dc microgrid's renewable energy sources and the energy storage component (the battery) was mainly built by LabVIEW mathematical modules (labVIEW Software Signal Express, 2012, National Instruments, Texas, USA 2012), based on equivalent circuits of the components. The detailed description of the model of each subsystem is given below.

2.1. Modeling of solar photovoltaic (PV) module

Solar PV panel equivalent circuit is shown in Fig. 1.

The output power from the solar PV panel at a specified output voltage is given as follows

$$P_{SOLAR} = V_{pv} I_{pv}. \tag{1}$$

The current supplied by the solar PV panel I_{pv} is given as follows

$$I_{pv} = \eta_p I_{ph} - \eta_p I_{rs} \left[\exp\left(\frac{q}{kTA} \frac{V_{pv}}{\eta_s} \right) - 1 \right] \tag{2}$$

where V_{pv} is output voltage of solar panels, I_{pv} is output current of solar panels, η_s is the number of solar panels in series, η_p is the number of solar panels in parallel, k is the Boltzmann constant, q is the electron charge, A is the ideality factor (ranges from 1 to 2), T is surface temperature of the solar panels (Kelvin), and I_{rs} is reverse saturation current, I_{ph} is the solar PV phase current expressed in Amp. (A) (Chen et al., 2013).

In (1), the characteristic of reverse saturation current I_{rs} varies with temperature as

$$I_{rs} = I_{rr} \left[\frac{T}{T_r} \right]^3 \exp\left(\frac{qE_q}{kA} \left(\frac{1}{T_r} - \frac{1}{T} \right) \right) \tag{3}$$

where T_r is the reference temperature of the solar panels (Kelvin), I_{rr} (A) is reverse saturation current of the solar panels at temperature T_r (Kelvin), and E_q is energy band gap of semiconductor material.

$$I_{ph} = [I_{scr} + \alpha (T - T_r)] \frac{S}{100} \tag{4}$$

where I_{scr} is the short circuit current at reference temperature T_r (Kelvin) and solar insolation specified at 0.85 kW/m^2, α is the short circuit current temperature coefficient of the solar panels, and S is the solar insolation (kW/m^2). The hourly values of input variables for modeling all the renewable energy sources are taken from smart grid pilot project commissioned at Mysore, India (http://indiasmartgrid.org/en/Lists/SmartGrid_Project/Attachments/9/14%20Smart%20Grid%20Pilots%20-%20Updates.pdf).

For this study we used Panasonic HIT-240S-BL solar modules each with a power rating of 240 W as the photovoltaic device of the microgrid system. This study used a solar system of 13 kW_p at M.P.P.T. (maximum power point tracking) generated by twenty photovoltaic arrays in parallel, where each array was built with twenty eight solar panels in series. This study used solar insolation of 0.85 kW/m^2 and constant temperature with varying V_{pv} for simulation verification.

2.2. Wind turbine modeling

The power generated by wind turbine is expressed as

$$P_{WIND} = 0.5 \rho A V^3 C_P (\tau_i, \theta) \tag{5}$$

where P_W is the power generated by the wind turbine W, ρ is the density of air in atmosphere (kg/m^3), A is cross-sectional area of a wind turbine blade (m^2), V is wind velocity (m/s), and C_P is the wind turbine energy conversion coefficient (Zhengming and Mingzong, 2010).

The density of air ρ (kg/m^3) and energy conversion coefficient C_P in (4) is expressed as

$$\rho = \left(\frac{353.05}{T} \right) \exp^{-0.034 \frac{Z}{T}} \tag{6}$$

$$C_P (\tau_i, \theta) = \left(\frac{116}{\tau_i} - 0.4 \times \theta - 5 \right) 0.5 \exp^{\frac{-16.3}{\tau_i}} \tag{7}$$

where Z is the altitude, T is the atmospheric temperature, τ_i is the tip speed ratio and θ is the blade tilt angle.

Table 1
Datasheet of input variables for RESs mathematical modeling modules.

Hour of the day	Avg. solar panel surface temperature (Kelvin)	Avg. wind speed (m/s)	Avg. biogas fuel consumption rate (m^3/h)
1	298.35	15.27784	0.000545
2	298.85	15.19444	0.000552
3	299.65	14.83333	0.000560.
4	300.95	14.52778	0.000562
5	301.35	14.19444	0.000567
6	303.35	13.78333	0.000597
7	305.95	12.85655	0.000602
8	306.95	13.38889	0.000604
9	308.35	13.19444	0.000608
10	309.85	13.30556	0.000611
11	310.65	13.87775	0.000637
12	311.85	10.41667	0.000689
13	311.35	09.02778	0.000717
14	310.95	11.66889	0.000734
15	308.85	12.80556	0.000789
16	305.55	11.78111	0.000811
17	304.45	09.87222	0.000834
18	303.65	10.34449	0.000875
19	302.55	11.89889	0.000938
20	301.45	10.74222	0.000973
21	300.55	09.53111	0.000758
22	299.35	08.88889	0.000648
23	298.25	07.77788	0.000597
24	298.35	15.27784	0.000545

The expression of the tip speed ratio τ_i in term of the initial tip speed ratio τ is given by

$$\tau_i = \frac{1}{\frac{1}{(\tau+0.089\theta)} - \frac{0.035}{(\theta^3+1)}} \tag{8}$$

$$\text{where} \quad \tau = r\frac{\omega}{V} \tag{9}$$

ω is the angular speed of the blade in revolution per second (rps) and r is the radius of the wind turbine blade in meter (m).
For this study we used JFNH-5kW wind turbine of Qingdao Jinfan Energy Science and Technology Co., Ltd. Wind speed is the most critical factor in wind power generation (Bharanikumar and Kumar, 2010).

2.3. Biogas fired ICE (internal combustion engines) model

The fuel consumption rate (m^3/h) of biogas fueled ICE is expressed as a quadratic function of real power:

$$F_{g,t} = a_g + b_g P_{g,t} + c_g P_{g,t}^2 \tag{10}$$

where $P_{g,t}$ is the gth generator output in kW at time t, a_g, b_g, c_g are coefficients that can be calculated from the datasheet provided by the manufacturer (http://power.cummins.com/onanpowerWeb/navigation.do?pageId=578).

The total fuel consumption rate F_t is given as follows:

$$F_t = \sum_{g=1}^{M} \left(a_g + b_g P_{g,t} + C_g P_{g,t}^2\right). \tag{11}$$

The ICE units are first constrained by their capacities:

$$P_g^- u_{g,t} < P_{g,t} < P_g^+ u_{g,t}, \quad \forall g \in M \tag{12}$$

where $P_g^{+,-}$ are the generator capacity lower bound and upper bound, $u_{g,t}$ is binary variable indicating the state of gth generator in time t (0 is off and 1 is on), M is the total number of generators.

The ICE units are constrained by minimum up and down time constraints

$$u_{g,s} \geq u_{g,t} - u_{g,t-1}, \quad \forall g, s \in \left(t+1, \ldots, t+UT_g - 1\right) \tag{13}$$

$$1 - u_{g,t} \geq u_{g,t-1} - u_{g,t}, \quad \forall g, s \in (t+1, \ldots, t+DT_g - 1) \tag{14}$$

where s is the time period, UT_g is the minimum up time of generator in hours, DT_g is the minimum down time of generator g in hours.

Ramp rate constraints are also considered for ICE units, which can restricts generator's output between two consecutive periods due to their physical limitations including start up and shut down periods:

$$P_{g,t} - P_{g,t-1} \leq R_g^+ u_{g,t-1} + R_g^{SU}\left(1 - u_{g,t-1}\right), \quad \forall g, t \tag{15}$$

$$P_{g,t-1} - P_{g,t} \leq R_g^- u_{g,t} + R_g^{SD}\left(1 - u_{g,t}\right), \quad \forall g, t \tag{16}$$

where $R_g^{+,-}$ are ramp up and ramp down constraints in kW when gth generator is on, $R_g^{SU,SD}$ are start up and shut down constraints in kW when gth generator starts up and shuts down.

Two other binary variables are used to represent start up and shut down states of ICEs as:

$$v_{g,t} = u_{g,t} - u_{g,t-1}, \quad \forall g, t \tag{17}$$

$$w_{g,t} = u_{g,t-1} - u_{g,t}, \quad \forall g, t \tag{18}$$

where $v_{g,t}$ and $w_{g,t}$ are binary variables indicating start up and shut down states of ICEs.
All the inputs variables to renewable energy sources mathematical modules are provided by separate datasheets prepared by taking average values of design parameters for each hour of the day recorded for Mysore microgrid pilot project in India and normalized over 24 h data points (http://indiasmartgrid.org/en/Lists/SmartGrid_Project/Attachments/9/14%20Smart%20Grid%20Pilots%20-%20Updates.pdf;). The same for day one is given below in Table 1.

2.4. Battery modeling

A Li-ion battery is an appropriate choice for high power application (Soloveichik, 2011). A series parallel connection of Li-ion battery would make a high power battery matrix, which can be used in our microgrid (Dogger et al., 2011).

The charge and discharge equations of the battery model are as follows:

$$I_c\left(it, i^*, i\right) = E_0 - k \cdot \frac{Q}{it + 0.1\,Q} \cdot i^*$$

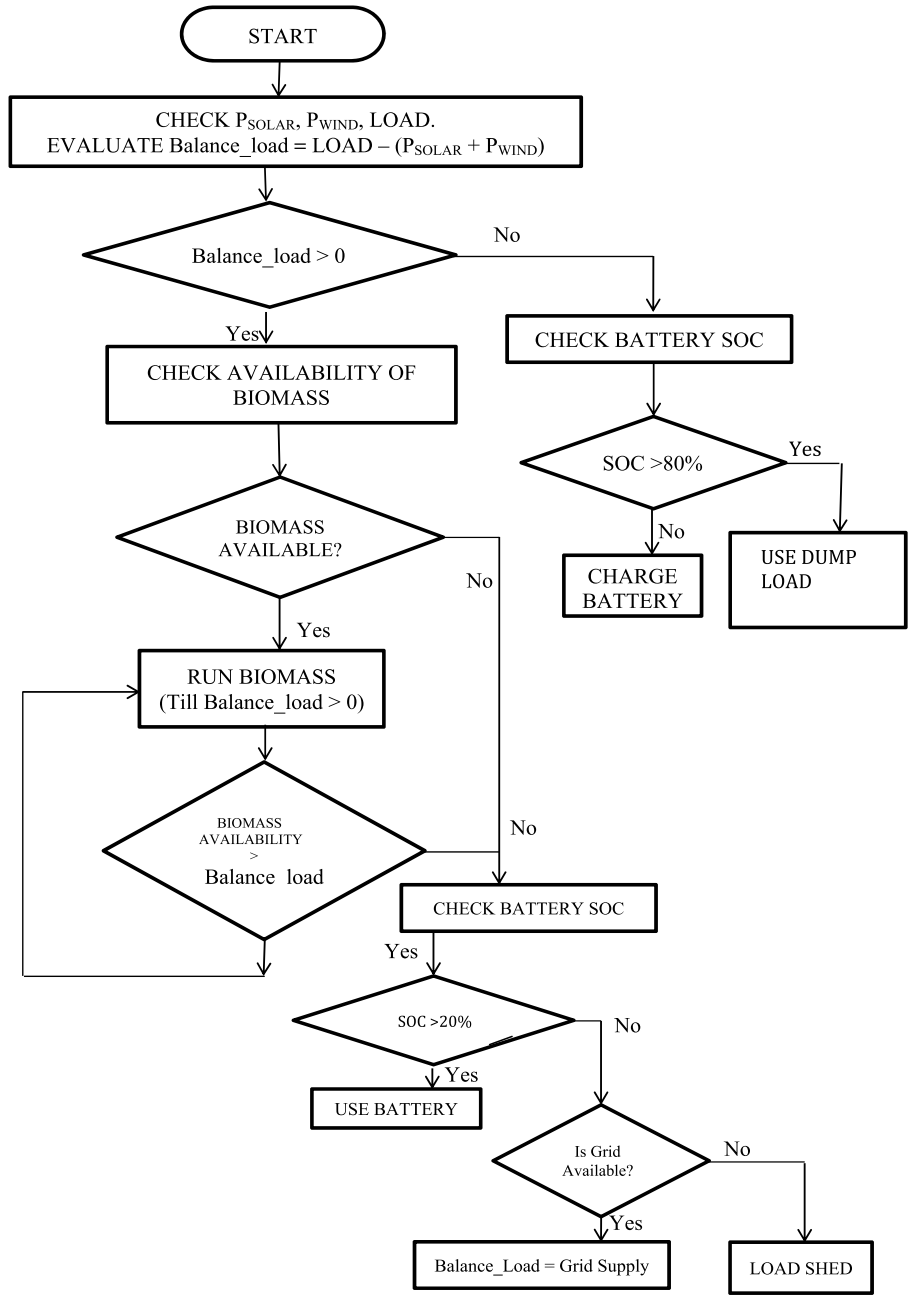

Fig. 2. Energy management algorithm flowchart.

$$-K \cdot \frac{Q}{Q-it} \cdot it + A \cdot \exp(-B \cdot it) \tag{19}$$

$$I_d\left(it,\ i^*, i\right) = E_0 - k \cdot \frac{Q}{Q-it} \cdot i^* - K \cdot \frac{Q}{Q-it} \cdot it + A \cdot \exp(-B \cdot it) \tag{20}$$

where E_0 is the initial voltage, K is the polarization resistance in ohms, i^* is the low-frequency dynamic current in Amps, i is the battery current in Amps., it is the battery extraction capacity (Ah), Q is maximum battery capacity (Ah), A is the exponential voltage, B is exponential capacity in $(\text{Ah})^{-1}$.

The SOC of the battery in the present model is calculated and updated using the following equation (Jiani et al., 2013).

$$\text{SOC}(t) = \text{SOC}(t_0) - \int_{t0}^{t} \frac{I_c(t) - I_d(t)}{C_n}\, dt \tag{21}$$

where C_n is battery's capacity, SOC (t_0) is the SOC at t_0 time, $I(t)$ is the battery current with discharging value as positive.

The battery module of 200 kWh proposed in this microgrid is an aggregation of 40,000 pieces of 4.1-V, 850-mAh TCL PL-383562 Li-ion battery cells similar to what was introduced in Chen and Rincon-Mora (2006).

3. Formulation of energy management algorithm

As shown in Fig. 2, the power outputs of the Solar panels and Wind farms are fetched by the MGCC from respective Remote Terminal Units (RTUs). The total connected load is also fed into the MGCC. Now the Balance_load is evaluated as:

$$\text{Balance\_load} = \text{Load} - (P_{SOLAR} + P_{WIND}). \tag{22}$$

Next, a comparison is made whether Balance_load is greater than zero or not. If Balance_load is not greater than zero, which means

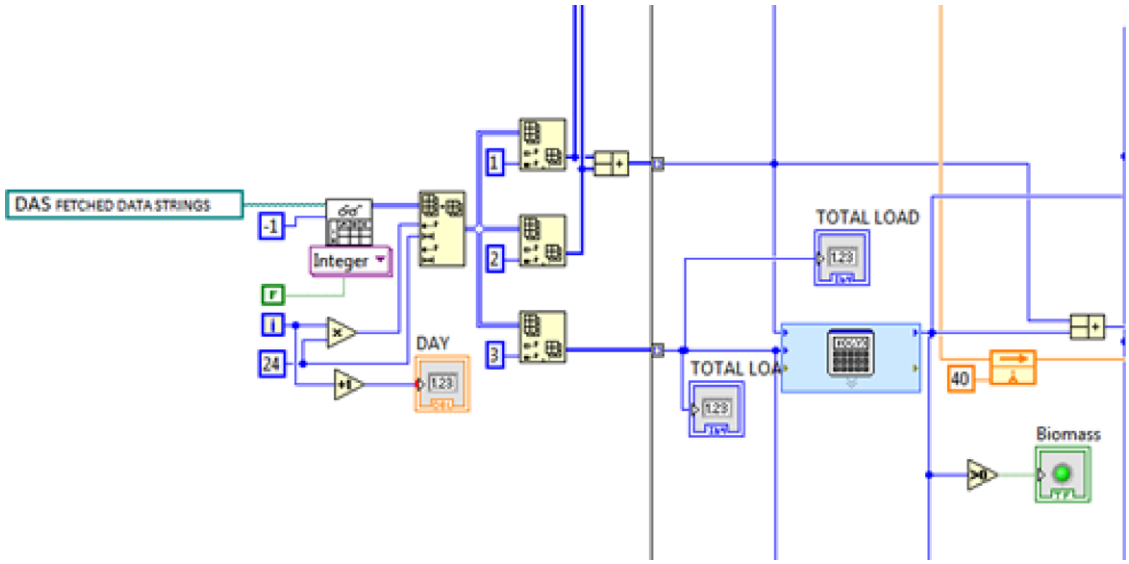

Fig. 3. Design for DAS fetched data bifurcation.

that the solar and wind power combined is more than the total connected load then the surplus power from the solar and wind energy sources has to be judiciously utilized. For this reason SOC of the battery is checked. If the SOC of the battery is less than 80% then we charge the battery with the surplus power. We do not charge the battery if the SOC is above 80% to avoid the possibility of damage.

In case the Balance_load is greater than zero, which means that the total load is greater than the combined power from solar and wind generations. In such a situation, the availability of the biogas is checked. If available, the biogas generator is run till the Balance_load is greater than zero. The MGCC checks whether the power available from biogas is greater than the Balance_load. If Biogas generated power is greater than the Balance_load then the biogas is run to meet the Balance_load till it is exhausted. If biogas generated power is insufficient to meet the Balance_load, the MGCC goes for the battery power insertion. In this case, the SOC of the battery is checked by MGCC through the inputs available from battery power measurement units. If the SOC of the battery is greater than 10% then we use the battery for supplying the Balance_load. In case if the SOC of the battery is not greater than 20% then MGCC will check for the Utility Grid availability for supplying the Balance_load. If the Utility Grid is available then it supplies the Balance_load but if it is not available then MGCC goes for load shedding by default.

4. Microgrid central controller (MGCC) design

The entire modeling and design of MGCC is based upon the above explained energy management algorithm shown in Fig. 2. This MGCC is designed on LabVIEW 2012 software of National Instruments (labVIEW Software Signal Express, 2012, National Instruments, Texas, and USA 2012). The structural design of the MGCC is divided into four parts. The DAS fetched Data bifurcation and mapping is done in first part as explained in Section 4.1. The Sections 4.2 and 4.3 explains the MGCC design related with the battery mechanism is initiated as per the implemented algorithm and calculation of its SOC respectively. The design that caters to the management of critical and non critical load is explained in the Section 4.4.

4.1. DAS fetched data bifurcation

As shown in Fig. 3, the data from different renewable energy sources and loads is sensed by respective sensors and is sent through low power radio (LPR) to the data acquisition system (DAS). DAS further sends the data to the microgrid central controller placed in the renewable energy management center over one of the many GPRS communication channels as per IEC standard IEC 61400-25 (wind energy) and IEC 61850-7-420 (solar PV).

MGCC first converts the data strings from different types of Renewable energy sources and loads fetched from DAS into an array of integers. This array of integers is mapped on a twenty-four hour basis string blocks of data structure divided into two parts of processed data. The first part consists of the processed data of wind energy and is sent to the wind energy management block and also to a adder function that counts for the total wind and solar power. The second part of processed data is the total solar energy, which is sent to the solar energy management block.

4.2. Battery initiation mechanism

As shown in Fig. 4, the Balance_load left to be met is expressed as the percentage of the total load in order to initiate the operation of the battery to supply the remaining load. The Formula2 shown in the dialog box in Fig. 4 is $(X2 - X1)/X2 * 100$. X1 represent the total renewable energy generation. The biogas generation is fed from the lower portion of the circuit block diagram. Now, the difference between the total renewable energy generation and the total load $(X2 - X1)$ divided by X2 gives us the percentage of the remaining load still left to be met. This value thus returned by the Formula2 block will initiate the battery mechanism.

4.3. State of charge estimation and battery functioning

The value returned from Formula2 is fed to a logical comparator shown in Fig. 5 whose second input is zero. The third input to this comparator is the biogas generation condition. This comparator will return a value computed by Formula2, if condition of the biogas insufficiency is true and it will return a value zero, if the condition of biogas generation insufficiency is false. Formula3 compares the state of charge of the battery to be greater than 20% or below 80%. X1 holds the value of SOC being fed from the SOC computational block in the lower section of the circuit block diagram that is mathematically modeled. First, the formula 3 computes the minimum of the battery SOC i.e. X1 and the numerical value 80 (upper limit of the battery SOC). Further this

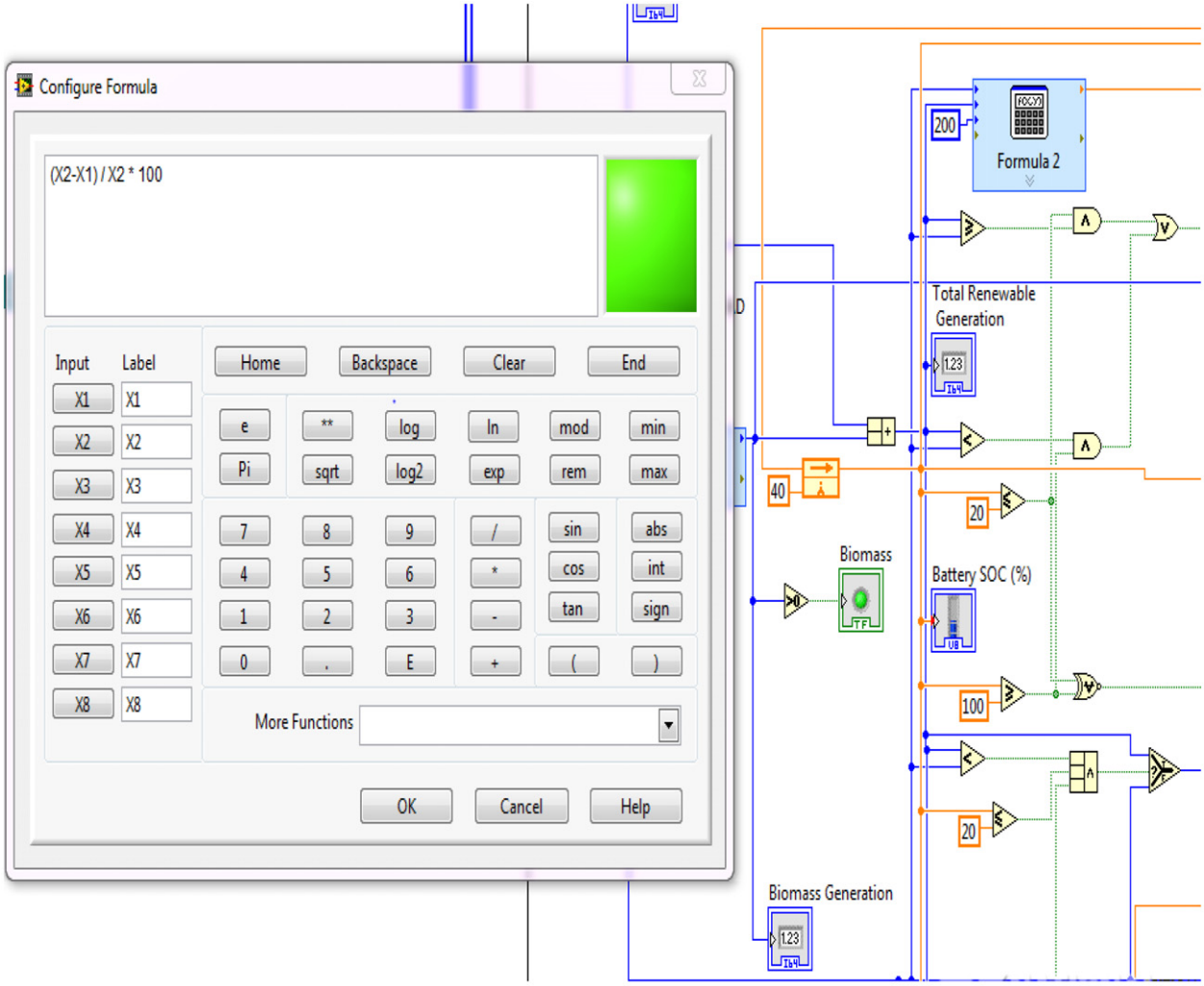

Fig. 4. Battery initiation mechanism.

formula computes the maximum of the SOC thus received and the numerical value 20 (lower limit of the battery SOC). Thus Formula3 returns the value of state of charge which may lie between 20% and 80%.

4.4. Load management block formulation

As shown in Fig. 6, the data of the state of charge of battery, the utility grid power and the Balance_load are fed as an input to the Compound Arithmetic Function block of the circuit diagram. The Balance_load will be subtracted from the available utility grid power only if the state of charge of battery is less than 20% (lower limit of SOC). Thus, a comparator is fed with two inputs, one being the SOC and other being the constant value of 20. If the SOC is less than 20% then the comparator will return 1 to actuate the Compound Arithmetic Function block. Its output is fed as an input to the 'select function block'. The 'select function block' takes the upper input as the total renewable energy generation, lower as the total load and middle as the actuating signal which is the Balance_load. It returns the value of the total load if the available grid power is less than the Balance_load and returns the value of the Balance_load if this condition is false. The output of this block gives the value of load that cannot be met by any available sources of energy upon the unavailability of grid power and thus has to be shed.

5. Results and discussion

The renewable energy management algorithm has been successfully implemented through the above discussed MGCC design. The simulations results show the accuracy of this implementation for the sustainable operation of microgrid.

5.1. Renewable energy generation pattern

The Renewable Energy generation pattern in Fig. 7 shows the simultaneous variation of wind, solar and biogas generation synchronized for 24 h of the day. It can be observed that during first 4 h of the day, there was no solar power till sunshine period started from 7 am but in this period there was some amount of wind power generation as ample wind velocity was available between 12:01 and 6 am (https://eosweb.larc.nasa.gov/cgi-bin/sse/subset.cgi?email=skip@larc.nasa.gov). It was observed that between 12:01 and 6 am the combined solar and wind generation was not sufficient enough to supply the total connected load. Thus, the remaining Balance_load [load− (solar + wind)] had to be met by the biogas energy generation as per the algorithm. It is obvious from the graph of biogas generation that the biogas generation was most active during 12:01–7 am by receiving the energy management signals from MGCC. The situation between 1 and 4 pm was that, the combination of solar and wind energy produced surplus power, which was be utilized for charging the battery. The situation

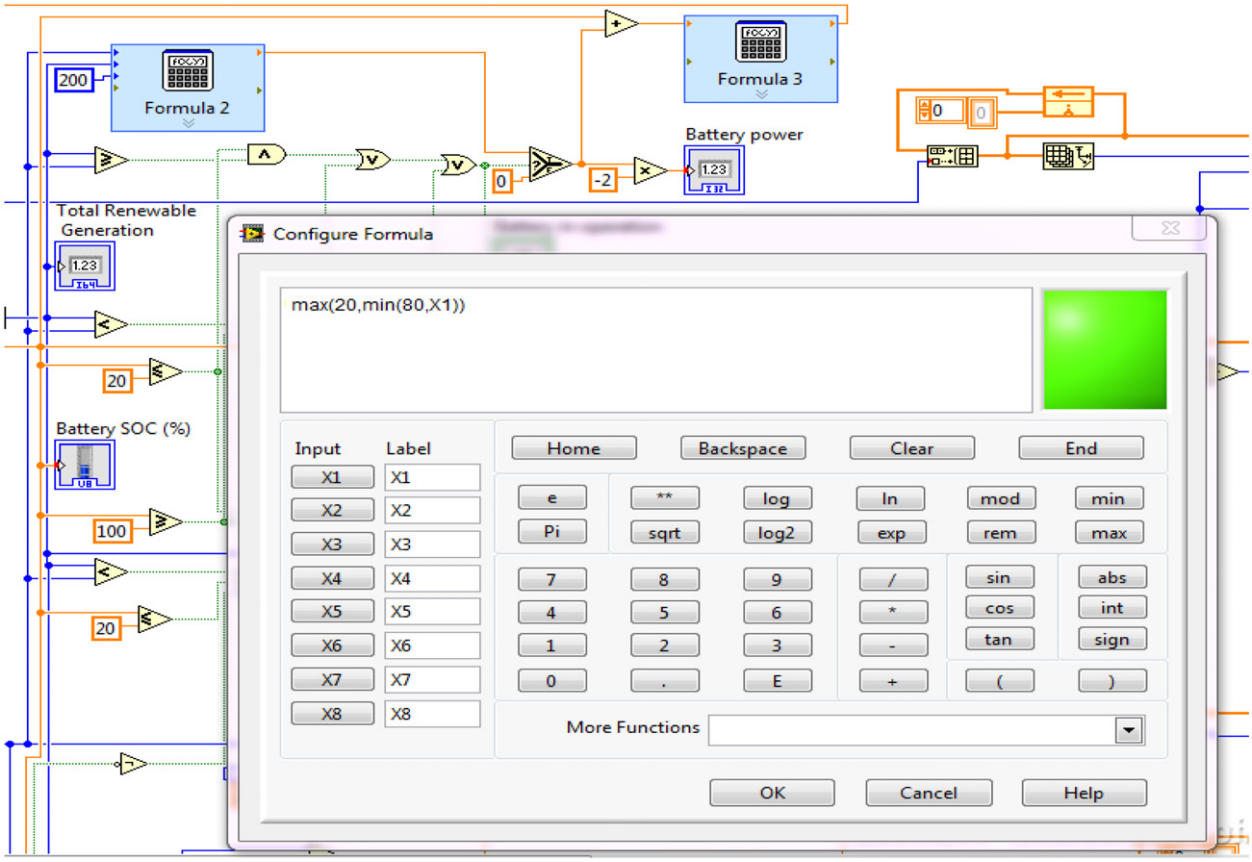

Fig. 5. State of charge estimation and battery functioning.

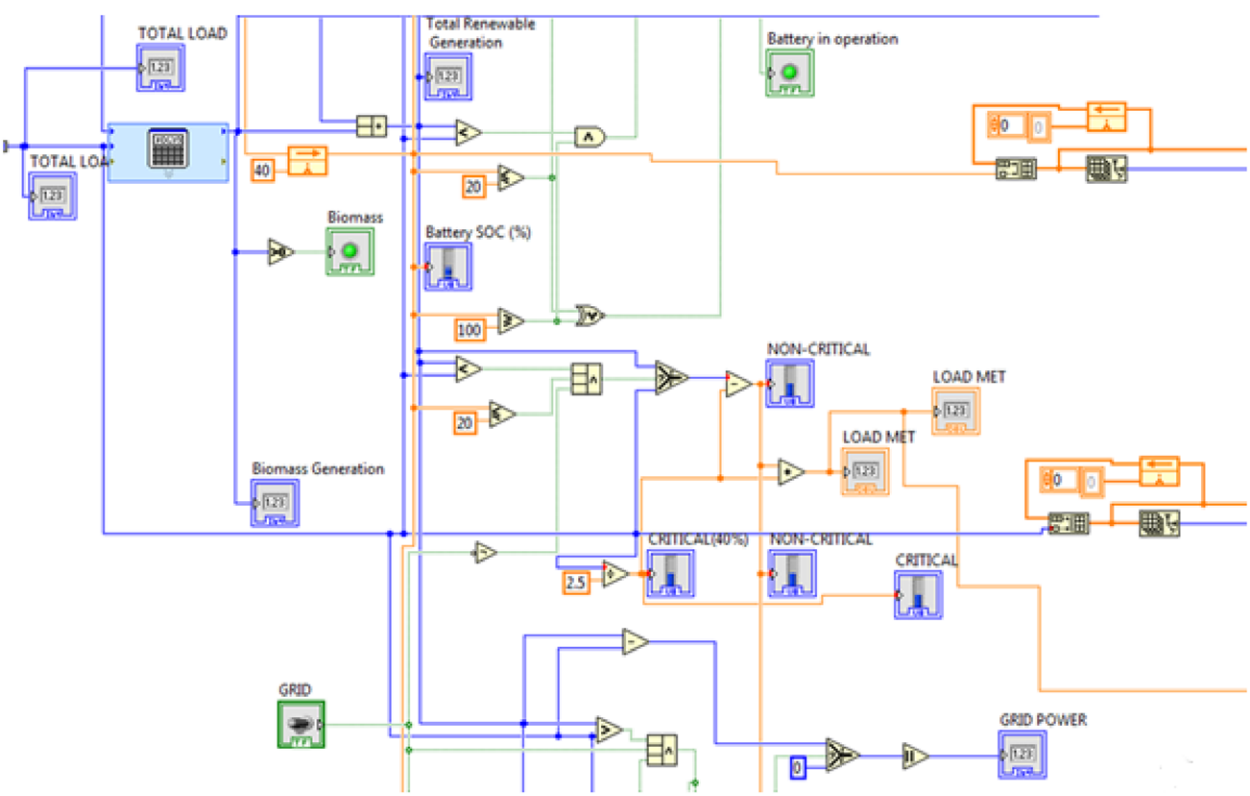

Fig. 6. Load management mechanism.

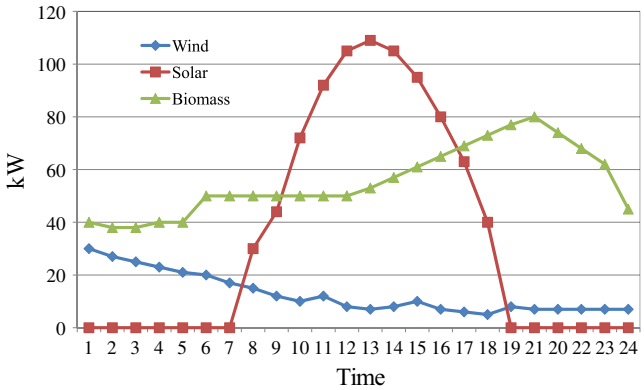

Fig. 7. Renewable energy generation pattern display.

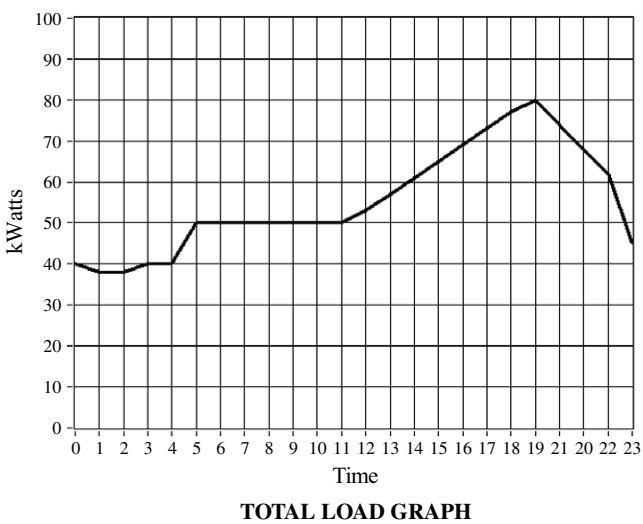

Fig. 8. Total load variation pattern display.

at 11 pm witnessed a lack of generation from all RESs and as SOC of the battery was less than 20%, utility grid power was injected to meet the Balance_load. The three synchronized renewable energy graphs supplying the net load clearly establish the operational success of this novel energy management algorithm and MGCC design.

5.2. Load variation pattern

As shown in Fig. 8, the load between 12:01 and 7 am was met primarily by wind energy and biogas. The load after 7 am was handled collectively by solar and wind power through MGCC control action. From 8:30 to 10 am the load was consistent, but due to a fall in wind generation and insufficiency of biogas energy, the battery (at SOC greater than 80%) supplied the Balance_load. The peak of this load curve occurred at around 7 pm in the evening when domestic housing load was most active and was met collectively by wind and biogas energy. From Figs. 7 and 8 we can observe the correct functioning of MGCC in managing the intermittent renewable energy sources in order to meet the connected load in a reliable manner.

6. Conclusion

This paper proposes an original renewable energy management algorithm for maintaining a sustainable power balance in the microgrid under consideration. This paper establishes the necessity of considering the status of various renewable energy sources and battery backup in a synchronized manner for the design of a microgrid central controller that is used to implement the proposed energy management algorithm. The MGCC has been developed based on multi agent system (MAS) concept in which data acquisition system (DAS) for the renewable sources and loads. The DAS consists of multiple sensors that are interconnected through Low Power Radio (LPR) to communicate with the control center as per IEC standard IEC 61400-25 (wind energy) and IEC 61850-7-420 (solar PV).

Since all the renewable sources are not available at the same time, a combination of various power sources should be deployed to meet the load depending upon the load demand during a particular period. To make the energy management system more reliable, a battery power control mechanism is implemented here. For the safe and reliable operation of the battery, its SOC is kept as an important constraint i.e. we do not charge it above 80% of SOC nor do we extract battery power to meet the load when its SOC is below 20%.

In order to get a satisfactory performance from the MGCC, a provision for the utility grid insertion has been made in the embedded algorithm in case all other energy options of proposed microgrid are exhausted. This increases the reliability of the microgrid as a whole.

References

Arulampalam, A., Barnes, M., Engler, A., Goodwin, A., Jenkins, N., 2004. Control of power electronic interfaces in distributed generation microgrids. Int. J. Electron. (91), 503–523.
Bharanikumar, R., Kumar, A.N., 2010. Analysis of wind turbine driven PM generator with power converter. Int. J. Comput. Electr. Eng. 2 (4), 766–769.
Bragard, M., Soltau, N., Thomas, S., De Doncker, R., 2010. The balance of renewable sources and user demands in grids: Power electronics for modular battery energy storage systems. IEEE Trans. Power Electron. 25 (12), 3049–3056.
Bull, S.R., 2001. Renewable energy today and tomorrow. Proc. IEEE 89 (8), 1216–1226.
Chen, M., Rincon-Mora, G., 2006. Accurate electrical battery model capable of predicting runtime and I-V performance. IEEE Trans. Energy Convers. 21 (2), 504–511.
Chen, Y.-K., Wu, Y.-C., Song, C.-C., Chen, Y.-S., 2013. Design and implementation of energy management system with fuzzy control for DC microgrid systems. IEEE Trans. Power Electron. 28 (4), 1563–1570.
Dogger, J., Roossien, B., Nieuwenhout, F., 2011. Characterization of li-ion batteries for intelligent management of distributed grid-connected storage. IEEE Trans. Energy Convers. 26 (1), 256–263.
Jiani, Du, Youyi, Wang, Changyun, Wen, 2013. Li-ion battery SOC estimation using particle filter based on an equivalent circuit model. In: Proc. 10th IEEE International Conference on Control and Automation, ICCA, Held in Hangzou China from 12–14 June, pp. 580–585.
Gaonkar, D.N., 2010. Investigation on electromagnetic transients of distributed generation systems in the microgrid. Electr. Power Compon. Syst. 38, 1486–1497.
Hledik, R., 2009. How green is smart grid? Electr. J. 22 (3), 29–30.
labVIEW Software Signal Express, 2012. National Instruments, Texas, USA 2012.
Xu, Ling, Miao, Zhixin, Fan, Lingling, 2012. Control of a battery system to improve operation of a Microgrid. In: Proc. IEEE on Power and Energy Society General Meeting held in San Diego, California, USA, During 22–26 July, pp. 1–8.
Mishra, S., Mallesham, G., Jha, A.N., 2012. Design of controller and communication for frequency regulation of a smart Microgrid. IET Renew. Power Gener. 6 (4), 248–258.
Prajapati, V., Hess, H., William, E.J., Gupta, V., Huff, M., Manic, M., Rufus, F., Thakker, A., Govar, J., 2011. A literature review of state of-charge estimation techniques applicable to lithium poly-carbon monoflouride (LI/CFx) battery. In: 2010 India International Conference on Power Electronics, IICPE, pp. 1–8, 28–30 January.
Soloveichik, G.L., 2011. Battery technologies for large-scale stationary energy storage. Annu. Rev. Chem. Biomol. Eng. 2 (1), 503–527.
Sovacool, B.K., 2008. Renewable energy: Economically sound, politically difficult. Electr. J. 21 (5), 18–29.
Valenciaga, F., Puleston, P.F., 2005. Supervisor control for a stand-alone hybrid generation system using wind and photovoltaic energy. IEEE Trans. Energy Convers. 20 (2), 398–405.
Vazquez, S., Lukic, S., Galvan, E., Franquelo, L., Carrasco, J., 2010. Energy storage systems for transport and grid applications. IEEE Trans. Ind. Electron. 57 (12), 3881–3895.
Xiong, Xiaofu, Ouyang, Jinxin, 2011. Modeling and transient behavior analysis of an inverter-based microgrid. Electr. Power Compon. Syst. 40, 112–130.
Zhengming, L., Mingzong, C., 2010. Small stand-alone wind turbine device characterstics analysis, vol. 35 (M.S. thesis), Electrical Engineering, Southern Taiwan University of Science and Technology, Tainan, Taiwan.
Miao, Zhixin, Xu, Ling, Disfani, V.R., Fan, Lingling, 2014. An SOC-based battery management system for microgrids. IEEE Trans. Smart Grid 5 (2), 966–973.